

LETTER • **OPEN ACCESS**

Imaging of hidden object using passive mode single pixel imaging with compressive sensing

To cite this article: Qi Chen *et al* 2018 *Laser Phys. Lett.* **15** 126201

View the [article online](#) for updates and enhancements.



IOP | ebooks™

Bringing you innovative digital publishing with leading voices to create your essential collection of books in STEM research.

Start exploring the [collection](#) - download the first chapter of every title for free.

Letter

Imaging of hidden object using passive mode single pixel imaging with compressive sensing

Qi Chen^{1,2}, Sandeep Kumar Chamoli^{2,3}, Peng Yin¹, Xin Wang²
and Xiping Xu^{1,2,4}

¹ College of Optoelectronic Engineering, Changchun University of Science and Technology, Changchun, Jilin 130022, People's Republic of China

² School of Engineering, Monash University Malaysia, Jalan Lagoon Selatan, 47500 Bandar Sunway, Selangor, Malaysia

³ The Guo China-US Photonics Laboratory, State Key Laboratory of Applied Optics, Changchun Institute of Optics, Fine Mechanics and Physics, Chinese Academy of Sciences, Changchun 130033, People's Republic of China

E-mail: 1551497786@qq.com

Received 4 August 2018

Accepted for publication 31 August 2018

Published 23 October 2018



CrossMark

Abstract

Hidden object imaging has always been challenging for obtaining satisfiable imaging because of the limitations caused by the reflections from the surrounding environment. The light is highly degraded after propagation and reflection from the hidden object. Single-pixel imaging (SPI) is an advanced imaging approach becoming more remarkable; applicable for acquiring spatial information in low light, high absorption and backscattering conditions. Combination of SPI and compressed sensing (CS) can efficiently tackle the key drawbacks of SPI, such as long data-acquisition time and low reconstruction resolution. In the present study, a CS based hidden object SPI system is designed. This is able to reconstruct an image without the influence of diffuse reflection from a two-dimensional (2D) target, which is placed in a corner practically concealing the objects over 10×10 cm of hidden space. The reconstruction obtained by our method is desirable and can save more than half of the data-acquisition time compared to the SPI algorithm. Our contribution presents a new insight for the application of SPI and provides a guideline for researchers to improve their applications.

Keywords: single pixel imaging, compressive sensing, image reconstruction, hidden object

(Some figures may appear in colour only in the online journal)

1. Introduction

Compared to traditional imaging, the imaging of scenes hidden from the camera's direct line of sight—known as seeing

around corners, or non-line-of-sight (NLoS) imaging—has attracted growing attention in recent years. Much research has been done aiming to detect, track and image hidden objects [1–8]. Single-pixel imaging (SPI) [9–11], a novel imaging technique by means of coincidence measurement, has proven that SPI can capture images in low light, high absorption and high backscattering conditions [12–14]. This unique feature efficiently makes it possible to capture the image of hidden objects. In a passive SPI system, a beam emitted from a light

⁴ Author to whom any correspondence should be addressed.



Original content from this work may be used under the terms of the [Creative Commons Attribution 3.0 licence](https://creativecommons.org/licenses/by/3.0/). Any further distribution of this work must maintain attribution to the author(s) and the title of the work, journal citation and DOI.

source illuminates the target and reflects to a digital micro-mirror device (DMD) after interacting with the objects. After processing by the DMD, the reflected light is focused on a photodetector to get the intensity values. Using this technique, images are reconstructed from a series of continuous measured intensity, each of them means an independent subset of the spatial information in the same scene. This makes imaging possible in a complex situation, which is impossible or challenging with multipixel image sensors.

Due to SPI advantages and the rapid development of spatial light modulators (SLMs), a lot of experimental setups have been built recently to capture imaging in different fields. Paul Nipkow might be the earliest researcher to use an SPI technique by means of a rotating Nipkow disk to encode and transmit image information in 1884 [15]. Based on SPI, a technique called optical coherence tomography has been developed by David *et al* for noninvasive cross-sectional imaging in biological systems [16]. Howland established a laser-based 3D imaging system by means of photon-counting and compressive sensing [17]. Howland used a single-pixel camera to realize a compressed sensing, photon counting lidar system and reconstructed both depth and intensity maps from a single under-sampled set of incoherence [18]. For the wavelengths where multipixel image sensors are unavailable, a lot of research has also been done using SPI, such as imaging in the terahertz band [19, 20] and fluorescence imaging through scattering media and multimode fibers [21–23].

However, there are limited studies focusing on the application of SPI to capturing images of hidden objects, and systematically investigating the influence of pattern types and measurements on the reconstruction performance. Therefore, exploiting advantages of SPI for hidden object imaging, we demonstrate a passive SPI imaging technique to reconstruct images of NLoS targets via diffusely reflected laser pulses. We design an experimental setup, which has the ability to recover the hidden object images. For the SPI algorithm, to completely capture the whole unknown scene up to a particular resolution, the least number of measurements required is equal to the total number of pixels in the reconstructed images [24]. Hence, a compressing technique is employed to reconstruct the image in order to save sampling time and improve the reconstruction efficiency in the current research. Our experimental results show that the proposed compressed sensing (CS)-based passive underwater SPI are more reliable than conventional imaging approaches for hidden objects. In addition, our method can save more than half of the time to get the same resolution, compared with SPI algorithm.

We begin with a brief theoretical introduction of underwater SPI in section 2. In section 3, we show the reconstructed images using various pattern types and the number of measurements. Moreover, evaluations of the performance with regard to each other and the original targets are also presented in this section. Finally, our conclusion and future work are given in section 4.

2. Theory

The SPI method acts by accumulating bucket sums of a light field that was both contacted with a target under investigation

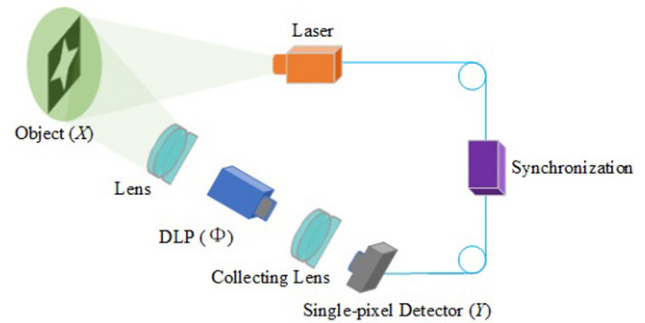


Figure 1. Schematic diagram of experimental setup: passive gated SPI system. DLP: digital light processing.

and a controllable modulator device. Practically, the way in which the imaging beam contacts with the object and the modulator (DMD) presents an essential difference between two unique approaches to the single pixel imaging method. It would be convenient to take the following approaches: the active mode is determined by following the agreement modulator, object and bucket detector; and the passive mode is determined by following an agreement object, modulator and bucket detector. Standard SPI system architecture contains the following main components: a source of light, optics, a single pixel detector and an SLM. Figure 1 shows the schematic of our experimental setup to detect and image the hidden objects using SPI. We represent a single measurement Y_j in a multiplexing scheme by the following expression:

$$Y_j = \sum_{i=1}^N \Phi_{ji} X_i, \quad (1)$$

or by the matrix equation

$$Y = \Phi X, \quad (2)$$

where Y is a column vector with M -elements representing M measurements, and Φ is the $M \times N$ measurement matrix, in which each row represents a pattern displayed on the SLM. For a well-conditioned measurement matrix [25] and the fully determined case, i.e. $M = N$, the reconstruction becomes linear and can be solved by a simple matrix equation: $X = \Phi^{-1} \times Y$ [26]. The image can be spatially multiplexed with many different types of measurement matrices.

It is widely believed that intensity-based imaging systems require pattern values that are confined to either 1 or 0—as physical masks or patterns—to either pass light to the detector or stop it. However, utilization of patterns with negative values yield lower noise [26], but it is generally only achievable with phase-sensitive measurements. Often, intensity-based imaging masks are approximated by adding two $[1, 0]$ masks and subtracting those that obtain a mask with $[1, 0, -1]$ or $[1, -1]$ values [27]. However, there are two significant disadvantages to the above approach: twice as many measurements are necessary, thus doubling the acquisition time; and the noise power increases because the variance is additive [28].

CS is a scheme for the simultaneous compression and sampling of sparse signals through incomplete, non-adaptive linear measurements [21–23, 29]. The evolution of CS theory has led to a great advantage in the SPI field. Considering the

sparsity of objects with respect to measure functions, their known basis or exact solutions for single pixel measurements; equation (1) can be achieved even in the situations where the number of measurements, M , are less than 20% of the number of object pixels, N . Following that, there exists an N -dimensional sparsifying basis Ψ ($\Psi = \{\psi_1, \psi_2, \dots, \psi_N\}$). The N -dimensional signal, X ($X = \{X_1, X_2, \dots, X_N\}$), is called K -sparse, which can be expressed as:

$$X = \Psi S \quad (3)$$

in which $K \ll N$ non-zero entries are contained in the $N \times 1$ vector S .

For the CS theory, it is stated that, when the signal (X) contains such a K -sparse basis, signal (X) can be reconstructed to more than $M = O(K \log N)$ incoherent linear measurements with a high probability:

$$Y = \Phi X = \Phi \Psi S. \quad (4)$$

Here Y is a $M \times 1$ measurement vector and Φ is a $M \times N$ measurement matrix, which is incoherent with the sparsifying matrix Ψ [30].

The matrix Φ is defined as the measurement matrix [30]. If the maximum magnitude of the elements of $\Phi \Psi$ is small, the incoherent property would be fulfilled [31]. When Φ is a random basis for an example scrambled block Hadamard ensemble, a pseudorandom sequence and Bernoulli binary vectors; this condition is achievable [32, 33].

Since the K -sparse sparsifying basis, Ψ , occurs in several signal types, such natural images are sparse in Fourier, DCT or wavelet domains; a property taken advantage of in compression standards like JPEG2000 and JPEG. The l_1 norm minimization using measurement Y can retrieve S (hence X) [34]:

$$\hat{a} = \arg \min \|a\|_1, \quad (5)$$

$$\text{subject to } Y = \Phi \Psi a, \quad (6)$$

where $\|a\|_1 = \sum_{i=1}^N |a_i|$ represents the l_1 norm of S . This type of optimization problem is known as a basis pursuit [34].

The gradient of the sparse image can be utilized by applying total variation (TV) minimization to the image. The discrete gradient for a digital image X , can be determined at pixel location x_{ij} [35]:

$$\begin{aligned} G_{ij} &= \begin{pmatrix} G_{h:ij}(X) \\ G_{v:ij}(X) \end{pmatrix} \\ G_{h:ij}(X) &= x_{i+1j} - x_{ij} \\ G_{v:ij}(X) &= x_{ij+1} - x_{ij}. \end{aligned} \quad (7)$$

The TV of X can be written as the sum of the magnitudes of $G_{ij}(X)$ at each location in X :

$$\text{TV}(X) = \sum_{ij} \sqrt{G_{h:ij}(X)^2 + G_{v:ij}(X)^2}. \quad (8)$$

Quadratic constraints of TV minimization have been proposed to yield more suitable visual quality than the l_1 optimization when retrieving images using noisy observations [35]

$$\min \text{TV}(X), \quad (9)$$

$$\text{subject to } \|\Phi X - Y\|_2 \leq \epsilon. \quad (10)$$

Candes *et al* concluded seven distinct data reconstruction optimization problems. The CS inverse problem has been solved using a proposed software package (l_1 -MAGIC) with CS measurements [36].

3. Experiment and analysis

In the above sections, we present a brief theoretical introduction of the SPI, CS and schematic of our experiment setup. Having demonstrated the SPI, CS and schematic of the system, we show imaging of the hidden object with a compressive method. There are well-developed mathematical techniques to reconstruct X from an underdetermined equation (1). Here we use a sequence of ordered binary randoms and Hadamard patterns as the measurement matrix Φ . In the SPI algorithm, the acquisition speed for image reconstruction is straightly proportional to the number of measurements. Utilizing a compressive technique minimizes the necessary number of measurements, which reduces the reconstruction and computational time. The influence of pattern type and number of measurements on the quality of reconstructed images are investigated in the experimental part. The principle behind the scheme of CS imaging can be summarized in equation (1), in which Y is an $M \times 1$ column vector, X is an image with N pixels and Φ is the measurement matrix with an $M \times N$ dimension. Using CS, we can reconstruct the image with a lower number of measurements than the number of pixels in the image, which is not possible in an SPI algorithm, an optimization method described in [37, 38].

3.1. Experimental setup

Our experimental setup is demonstrated in figure 2. The laser source is required to illuminate the required area of the object using a collimator as it expands the laser beam diameter. After passing through the beam splitter (BS), the beam is split into two perpendicular directions. One beam goes to the glossy wall and a fraction of the beam goes towards the photodetector, which is connected to a delay generator and necessary to synchronize the laser beam with a single pixel detector. The reflected beam from the glossy wall is expected to interact with the hidden object, which has a glossy nature. After interacting with the object, the light beam is reflected from the wall again. Finally, the beam is projected onto a DMD chip through the BS and imaging lens. Using focused light from the imaging lens, random and Hadamard patterns are projected by the DMD to the collecting lens and focused onto the single pixel detector. The corresponding intensity values are captured by the DAQ.

The DLP (DLP Light Crafter 6500, Texas Instruments) is comprised of square micromirrors (1920 rows and 1080 columns), each mirror can be situated at two angles: $+12^\circ$ and -12° . Each mirror represents an individual pixel in X

and Φ . The orientation of each mirror can be either towards a collecting lens (representing 1 in Φ) or away from the collecting lens (representing 0 in Φ). The reflected light is focused onto the single pixel detector using a collecting lens, where it calculates the product of $X \Phi$ to measure the Y as an output voltage. The custom software was written in a matrix laboratory (MATLAB). With the plan of applying compressive sensing, the DLP is required to communicate with MATLAB so that the projection mask can be evolved in the middle of the measurement. Thus, a MATLAB code to communicate with the DLP through transmission control protocol/internet protocol has been introduced. Apart from DLP, DAQ is required to be linked with MATLAB as well. The data acquisition toolbox for MATLAB has already included the function ready to use with the National Instrument device. With the successful communication of the two devices, a MATLAB code was written to automate and, most importantly, synchronize the data collection procedure. It eliminates the possibility of linking the wrong reading to the mask. Instead of time-based correspondence, the DLP will only project the next matrix pattern after the reading for the current matrix pattern is acquiesced. With the elimination of the possible error, the measurements can be done at a faster pace and be more systematic. Following minimization of the total variation (min-TV), the reconstructed images can be realized within 20s of the reconstruction algorithm in MATLAB [37].

To evaluate the influence of pattern types on imaging quality, we employ peak signal-to-noise-ratio (PSNR), which is often used to measure the reconstruction quality of images. Here, PSNR is defined as:

$$\text{PSNR} = 10 \cdot \log_{10} \left(\frac{\text{MAX}_I^2}{\text{MSE}} \right) \quad (11)$$

where, MAX_I^2 is the maximum possible pixel value of the image when the pixels are represented using 8 bits per sample, this is 255 and MSE is the average squared difference between the estimated images and the original object which can be given by:

$$\text{MSE} = \frac{1}{mn} \sum_{i=0}^{m-1} \sum_{j=0}^{n-1} [R(i,j) - O(i,j)]^2, \quad (12)$$

in which $R(i,j)$ is the reconstructed image and $O(i,j)$ is the image of the object. In addition, $m \times n$ is the number of pixels in the comparison image.

3.2. Results and analysis

3.2.1. Influence of pattern. The characteristics and types of different spatially arranged patterns directly affect the imaging results in terms of possible resolution, fidelity, imaging speed and compressibility. Binary (Hadamard and random) patterns are used in our study to reconstruct the object. These patterns provide large spatial frequency information of the scene. In binary patterns, every pixel must be either fully transmissive (1) or not-transmissive (0). On the other hand, in the case of

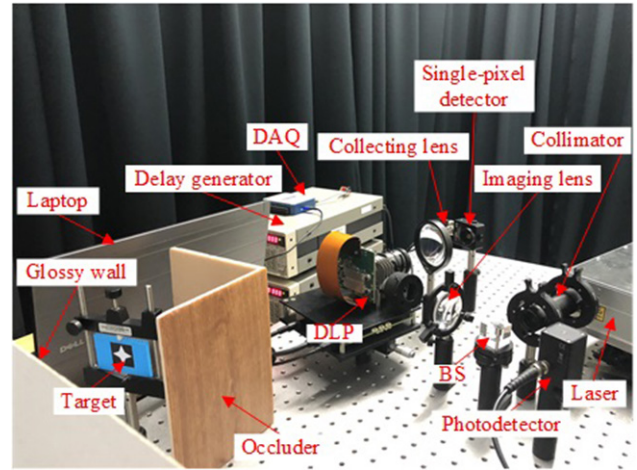


Figure 2. Experimental setups for hidden object SPI.

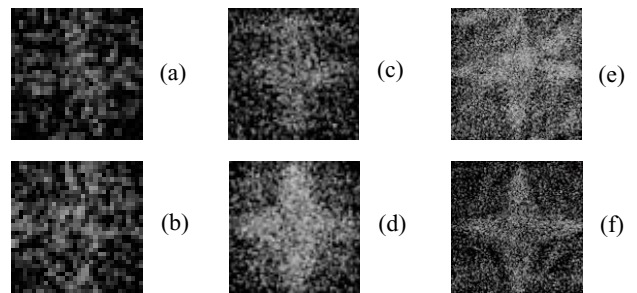


Figure 3. Reconstructed results with different resolution using random and Hadamard patterns under 1000 measurements. (a) 32×32 random pattern; (b) 32×32 Hadamard pattern; (c) 64×64 random pattern; (d) 64×64 Hadamard pattern; (e) 128×128 random pattern; (f) 128×128 Hadamard pattern.

grayscale patterns, the transmission of every pixel must vary between 0 and 1.

To examine the influence of patterns on reconstruction performance, images are reconstructed by projecting Hadamard and random patterns with varying resolutions (32×32 , 64×64 and 128×128) under same number of measurements. Figure 3(e) and (f) display the reconstructed 128×128 images of the hidden object by projecting random and Hadamard patterns under 500 measurements. From figure 3(f), the edges can clearly be seen using Hadamard patterns—other than the random one, which proves the quality with the Hadamard patterns are better. From all the reconstructed results in figure 3, it is evident that reconstruction is better for each resolution using the Hadamard pattern. Applying equations (11) and (12), the PSNR of the reconstructed images in figure 3 are calculated and plotted in figure 4. A clear rising trend of PSNR from 32×32 to 128×128 can be observed and the PSNR corresponding to the Hadamard pattern has a better response than the random pattern.

3.2.2. Influence of number of measurements. To investigate the effect of the number of measurements on hidden object imaging, images with different resolutions are reconstructed by projecting Hadamard patterns using varying number of measurements (300, 500 and 1000 measurements). The images obtained under nine different parameters are shown

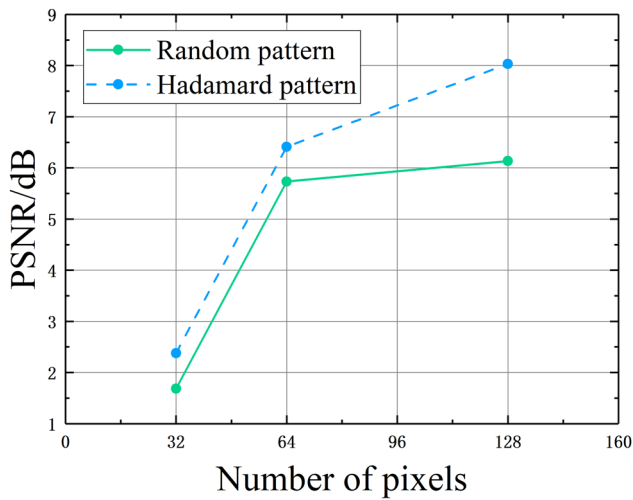


Figure 4. The plot of PSNR with different resolution under 1000 measurements with respect to projected pattern types.

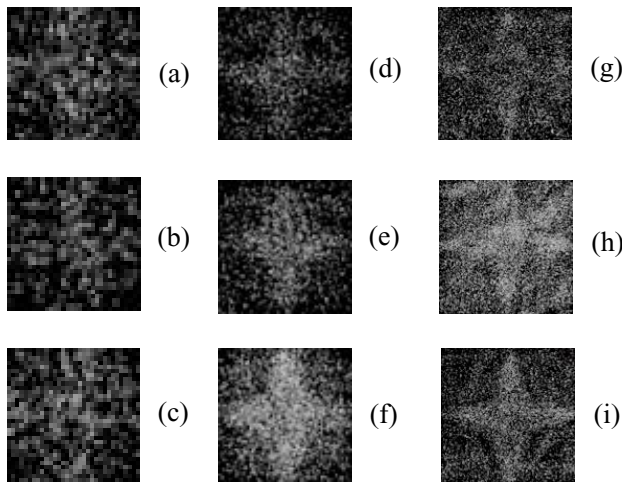


Figure 5. Reconstructed results with different resolution using Hadamard patterns under different number of measurements. (a) 32×32 300 measurements; (b) 32×32 500 measurements; (c) 32×32 1000 measurements; (d) 64×64 300 measurements; (e) 64×64 500 measurements; (f) 64×64 1000 measurements; (g) 128×128 300 measurements; (h) 128×128 500 measurements; (i) 128×128 1000 measurements.

in figure 5. During the sampling of the object, a fraction of the fine detail is missing because of the noise under sampling. The object can be reconstructed when the number of measurements is less than 20% of the total number of pixels using CS.

Based on figures 5(g)–(i), it is evident that the reconstructed images become more reliable on the increasing number of measurements from 300 to 1000 because the structure of the original object can be clearly detected with naked eyes. From figure 6, it can be observed that figures 5(c), (f) and (i) are the most reliable reconstructed images with different resolutions. The corresponding PSNRs of each reconstructed image of figure 5 are shown in figure 6, in which it is shown that the PSNR is proportional to the number of measurements. It can be observed that the reconstruction performance is higher for more measurements as compared to fewer measurements. The reconstructed image quality continually increases with the growth of the number of measurements. In general, we

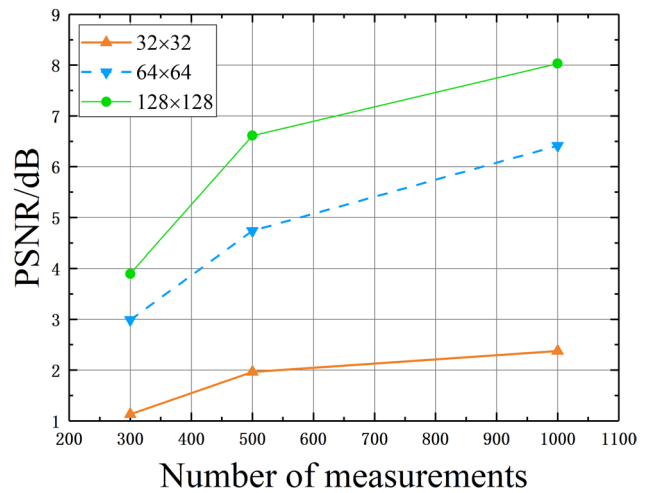


Figure 6. The plot of PSNR with different resolution under Hadamard patterns with respect to number of measurements.

can conclude that the more measurements we do, the higher reconstructed images we obtain. Therefore, more sampling times should be performed to obtain better reconstruction performance in real applications.

4. Conclusion and future work

In the current research, we designed a system to exhibit the novel application of SPI to image the hidden object, which is beneficial for practical applications of hidden object imaging. The proposed system employs Hadamard and random illumination patterns to reconstruct the 2D object image using CS. Following the CS approach, our system is capable to reconstruct the object with resolutions of 32×32 , 64×64 , and 128×128 using few measurements. Experimental results show that the reconstruction performance is proportional to the number of measurements. Therefore, to enhance reconstruction quality, a greater number of measurements are required. This substantial reduction in the number of measurements efficiently minimizes the data acquisition. The significant beneficial effects of Hadamard patterns compared with random patterns on object reconstruction have been shown in this paper.

In future, to extend our investigation of hidden object SPI, we will study the influence of factors such as laser wavelength, target characteristics, laser intensity and required optics on imaging performance.

Acknowledgments

This work was supported by the National Natural Science Foundation of China (NSFC) (61605016); Project 111 (D17017).

References

- [1] Xu F, Shulkind G, Thrampoulidis C, Shapiro J H, Torralba A, Wong F and Wornell G W 2018 Revealing hidden scenes by

- photon-efficient occlusion-based opportunistic active imaging *Opt. Express* **26** 9945–62
- [2] Velten A, Willwacher T, Gupta O, Veeraraghavan A, Bawendi M G and Raskar R 2012 Recovering three-dimensional shape around a corner using ultrafast time-of-flight imaging *Nat. Commun.* **3** 745
- [3] Valzania L, Zolliker P and Hack E 2017 Topography of hidden objects using THz digital holography with multi-beam interferences *Opt. Express* **25** 11038
- [4] Javidi B and Kishk S 2003 3D object watermarking by a 3D hidden object *Opt. Express* **11** 874–88
- [5] Janassek P, Blumenstein S and Elsässer W 2018 Recovering a hidden polarization by ghost polarimetry *Opt. Lett.* **43** 883
- [6] Gariepy G, Tonolini F, Henderson R, Leach J and Faccio D 2016 Detection and tracking of moving objects hidden from view *Nat. Photon.* **10** CTh4B.3
- [7] Cua M, Zhou E H and Yang C 2017 Imaging moving targets through scattering media *Opt. Express* **25** 3935
- [8] Cheng Q, Tan Z, Wang H and Wang G P 2017 Long distance invisibility system to hide dynamic objects with high selectivity *Sci. Rep.* **7** 10231
- [9] Zhang Z, Wang X, Zheng G and Zhong J 2017 Fast Fourier single-pixel imaging via binary illumination *Sci. Rep.* **7** 12029
- [10] Higham C F, Murraysmith R, Padgett M J and Edgar M P 2018 Deep learning for real-time single-pixel video *Sci. Rep.* **8** 2369
- [11] Augustin S, Frohmann S, Jung P and Hübers H W 2018 Mask responses for single-pixel terahertz imaging *Sci. Rep.* **8** 4886
- [12] Schmitt K M and Rahm M 2016 Evaluation of the impact of diffraction on image reconstruction in single-pixel imaging systems *Opt. Express* **24** 23863
- [13] Ren H, Zhao S and Gruska J 2018 Edge detection based on single-pixel imaging *Opt. Express* **26** 5501
- [14] Jauregui-Sánchez Y, Soldevila F, Clemente P, Tajahuerce E and Lancis J 2017 *European Conf. on Biomedical Optics SPIE Proc.* **10416** 104160C
- [15] Zhang Z, Wang X, Zheng G and Zhong J 2017 Hadamard single-pixel imaging versus Fourier single-pixel imaging *Opt. Express* **25** 19619–39
- [16] Huang D, Swanson E A, Lin C P, Schuman J S, Stinson W G, Chang W, Hee M R, Flotte T, Gregory K and Puliafito C A 1991 Optical coherence tomography *Science* **254** 1178–81
- [17] Howland G A, Dixon P B and Howell J C 2011 Photon-counting compressive sensing laser radar for 3D imaging *Appl. Opt.* **50** 5917–20
- [18] Lum D J, Howland G A, Howell J C and Ware M R 2013 Photon counting compressive depth mapping *Opt. Express* **21** 23822–37
- [19] Watts C M, Shrekenhamer D, Montoya J, Lipworth G, Hunt J, Sleasman T, Krishna S, Smith D R and Padilla W J 2014 Terahertz compressive imaging with metamaterial spatial light modulators *Nat. Photon.* **8** 605–9
- [20] Ivanov S R, Sun B, Hornett S M, Hobson P A, Gibson G M, Padgett M J and Euan H 2016 Noninvasive, near-field terahertz imaging of hidden objects using a single-pixel detector *Sci. Adv.* **2** e1600190
- [21] Popoff S M, Goetschy A, Liew S F, Stone A D and Cao H 2014 Coherent control of total transmission of light through disordered media *Phys. Rev. Lett.* **112** 1–2
- [22] Plöschner M, Tyc T and Čížmár T 2015 Seeing through chaos in multimode fibres *Nat. Photon.* **9** 529–35
- [23] Mahalati R N, Gu R Y and Kahn J M 2013 Resolution limits for imaging through multi-mode fiber *Opt. Express* **21** 1656–68
- [24] Phillips D B, Sun M J, Taylor J M, Edgar M P, Barnett S M, Gibson G M and Padgett M J 2017 Adaptive foveated single-pixel imaging with dynamic supersampling *Sci. Adv.* **3** e1601782
- [25] Cheney W and Kincaid D 2007 *Numerical Mathematics and Computing* (Pacific Grove, CA: Brooks/Cole)
- [26] Harwit M 1979 *Hadamard Transform Optics* (New York: Academic)
- [27] Davis D S 1995 Multiplexed imaging by means of optically generated Kronecker products: 1. The basic concept *Appl. Opt.* **34** 1170–6
- [28] Taylor J R 1982 *An Introduction to Error Analysis* (Mill Valley, CA: University Science Books)
- [29] Stantchev R I, Sun B, Hornett S M, Hobson P A, Gibson G M, Padgett M J and Hendry E 2016 Noninvasive, near-field terahertz imaging of hidden objects using a single-pixel detector *Sci. Adv.* **2** e1600190
- [30] Baraniuk R 2008 *Conf. on Information Sciences and Systems*
- [31] Candès E and Romberg J 2006 Sparsity and incoherence in compressive sampling *Inverse Problems* **23** 969–85
- [32] Gan L, Do T T and Tran T D 2015 *European Signal Processing Conf., 2008*
- [33] Do T T, Tran T D and Lu G 2008 *IEEE Int. Conf. on Acoustics, Speech and Signal Processing*
- [34] Chen S S, Donoho D L and Saunders M A 2001 Atomic decomposition by basis pursuit *SIAM Rev.* **43** 129–59
- [35] Candès E J, Romberg J K and Tao T 2006 Stable signal recovery from incomplete and inaccurate measurements *Commun. Pure Appl. Math.* **59** 1207–23
- [36] Smith G W, Beutler D E, Bell J D, Seymour C L G, Hohlfelder R J, Gallegos R R and Dudley J 2005 Novel x-ray imaging diagnostics of high-energy nanosecond pulse accelerators *Proc. SPIE* **5580** 559–71
- [37] Donoho D L 2006 Compressed sensing *IEEE Trans. Inf. Theory* **52** 1289–306
- [38] Candès E, Romberg J and Tao T 2006 Robust uncertainty principles: Exact signal reconstruction from highly incomplete frequency information *IEEE Trans. Inf. Theory* **52** 489–509